

# Model-agnostic explainable artificial intelligence for object detection in image data

Milad Moradi\*

AI Research, Tricentis, Vienna, Austria

m.moradi-vastegani@tricentis.com

Ke Yan

AI Research, Tricentis, Sydney, Australia

k.yan@tricentis.com

David Colwell

AI Research, Tricentis, Sydney, Australia

d.colwell@tricentis.com

Matthias Samwald

Institute of Artificial Intelligence, Center for Medical Statistics, Informatics, and Intelligent Systems,  
Medical University of Vienna, Vienna, Austria

matthias.samwald@meduniwien.ac.at

Rhona Asgari

AI Research, Tricentis, Vienna, Austria

r.asgari@tricentis.com

---

\* Corresponding author. **Postal address:** Tricentis GmbH, Leonard-Bernstein-Straße 10, 1220 Vienna, Austria.

## Abstract

---

In recent years, deep neural networks have been widely used for building high-performance Artificial Intelligence (AI) systems for computer vision applications. Object detection is a fundamental task in computer vision, which has been greatly progressed through developing large and intricate deep learning models. However, the lack of transparency is a big challenge that may not allow the widespread adoption of these models. Explainable artificial intelligence is a field of research where methods are developed to help users understand the behavior, decision logics, and vulnerabilities of AI systems. Previously, few explanation methods were developed for object detection, based on the idea of random masks. However, random masks may raise some issues regarding the actual importance of pixels within an image. In this paper, we design and implement a black-box explanation method named **Black-box Object Detection Explanation by Masking (BODEM)** through adopting a hierarchical random masking approach for AI-based object detection systems. We propose a hierarchical random masking framework in which coarse-grained masks are used in lower levels to find salient regions within an image, and fine-grained mask are used to refine the salient regions in higher levels. Experimentations on various object detection datasets and models showed that BODEM can be effectively used to explain the behavior of object detectors. Moreover, our method outperformed Detector Randomized Input Sampling for Explanation (D-RISE) with respect to different quantitative measures of explanation effectiveness. The experimental results demonstrate that BODEM can be an effective method for explaining and validating object detection systems in black-box testing scenarios.

---

**Keywords:** Explainable artificial intelligence, Deep learning, Computer vision, Object detection, Hierarchical masking, Black-box testing

# 1. Introduction and background

Artificial Intelligence (AI) and Machine Learning (ML) methods have been widely used in recent years for building intelligent systems, which can accurately perform automatic tasks that require human intelligence (Devlin, Chang, Lee, & Toutanova, 2018; Jordan & Mitchell, 2015; LeCun, Bengio, & Hinton, 2015; Radford et al., 2019; Russell & Norvig, 2009). Deep Neural Networks (DNNs) have had a major contribution in the success of AI systems, due to their great abilities in capturing complex data relationships. DNNs trained on sufficiently large datasets can then be used as either high-performance generative or discriminative ML models. A generative ML model captures the joint probability of the data and the target in a supervised scenario, or the distribution of the data itself in an unsupervised scenario. Generative models can be used to extract patterns from large datasets or to generate new samples that look like real data. On the other hand, a discriminative ML model captures the conditional probability of the data and the target. Discriminative modelling is usually used to build predictive ML models that perform common predictive tasks such as classification and regression. Both generative and discriminative approaches have found various applications in pattern recognition, computer vision, natural language processing, speech recognition, and recommender systems (Weibo Liu et al., 2017).

A DNN consists of a hierarchical architecture of layers, with each layer containing multiple non-linear processing units. When training a DNN, lower layers (i.e. layers that are closer to the input) usually learn simpler data relationships and pass them to the next layers. As the input passes through DNN layers, more complex patterns are learned, building on simpler patterns learned by the previous layers. Upper layers of a DNN, which are closer to the final output, usually act as functions that approximate the target output that is specified by the task at hand. Multi-layer perceptrons, deep belief networks, autoencoders, Convolutional Neural Networks (CNNs), Recurrent Neural Networks (RNNs), and transformers are the most commonly used DNN architectures with various applications in image, text, time series, and tabular data processing (Khamparia & Singh, 2019; LeCun et al., 2015; Weibo Liu et al., 2017).

CNN is a popular DNN architecture inspired by the organization of the natural visual perception of living creatures (Gu et al., 2018). CNNs can be ideal models for extracting patterns from multi-dimensional data with grid-like topology, e.g. images and videos. Convolutional layers in a CNN convolve their input with trainable filters at all possible receptive fields, resulting in local feature maps. Using pooling layers, subsampling is then performed on the feature maps to reduce their size. As the input passes through multiple convolutional and subsampling layers, higher level transformations of the input are constructed. Finally, after rasterizing, which

represents the final feature map as a one-dimensional vector, the output of the CNN is fed into one or more fully-connected layers to produce the final output.

CNNs have various applications in computer vision and image processing (Gu et al., 2018; Li, Liu, Yang, Peng, & Zhou, 2022). They can effectively help AI systems gain high-level understanding from digital images and detect complex structures. A CNN is composed of simple but non-linear modules, which learn multiple levels of abstraction in multiple layers of the neural network. The input of the first layer comes in the form of arrays of pixel values in different Red, Green, and Blue (RGB) channels, or other colour models. The representations learned by the first layer typically encode the presence or absence of edges with particular orientation at specific locations in the image. The subsequent layers usually detect particular combinations of edges and encode motifs into feature maps, and then identify parts of familiar objects as a result of combining motifs. Finally, the last layers detect objects through assembling those parts identified by the previous layers (LeCun et al., 2015).

Object detection is a fundamental task in image processing, whose goal is to localize and classify objects in an image (Zaidi et al., 2022). Object detection can provide essential information for semantic understanding of images and videos, which has applications in autonomous driving, image classification, face recognition, and other related tasks (Zhao, Zheng, Xu, & Wu, 2019). With the emergence of DNNs, we have witnessed considerable performance improvement in computer vision applications, especially object detection. CNNs typically form the backbone of object detection systems and serve as feature detectors (Jiao et al., 2019). Regions with CNN (R-CNN) (Girshick, Donahue, Darrell, & Malik, 2014), Fast R-CNN (Girshick, 2015), Faster R-CNN (Ren, He, Girshick, & Sun, 2015), Mask R-CNN (He, Gkioxari, Dollár, & Girshick, 2017), You Only Look Once (YOLO) (Redmon, Divvala, Girshick, & Farhadi, 2016), and Single-Shot Detector (SSD) (Wei Liu et al., 2016) are among the most popular object detection models.

In spite of deep learning methods' impressive success, the lack of interpretability has been a barrier to the widespread adoption of these methods, especially in mission-critical applications (Guidotti et al., 2018). In order to trust an ML model, users need to be able to explain or interpret what the model has learned (Murdoch, Singh, Kumbier, Abbasi-Asl, & Yu, 2019). It is easier to trust an ML model's decisions, detect its potential biases, take actions to refine it, and optimize its performance when we have a clear understanding of the model, its behaviour, and its vulnerabilities (Moradi & Samwald, 2021b, 2021c, 2022).

Explainable AI (XAI) is a field of research where methods are studied and developed to provide users with the ability of understanding, explaining, and interpreting AI and ML systems (Adadi & Berrada, 2018). There are several examples of black-box AI models whose decisions

were revealed to be biased or unfair after explaining them (Guidotti et al., 2018). In computer vision, XAI has also helped to discover biases and failure points of DL models utilized for object detection and classification (Freitas, 2014; Ribeiro, Singh, & Guestrin, 2016). XAI methods for computer vision can be divided into two categories, i.e. white-box and black-box, based on their access to the DL model's internals. White-box methods have access to information about the underlying DL network, such as its architecture, loss function, activation functions, connection weights, or training data. On the other hand, a black-box XAI method has no access to such information; it only knows about the input sample and the final output generated by the DL model. A big challenge of white-box methods is that we do not always have access to the model's internals. Moreover, only AI experts may be able to interpret those explanations derived from the model's internals. In applications where we are interested in understanding the behaviour of the AI model and discovering its vulnerabilities, e.g. in **software testing** (Ammann & Offutt, 2016), black-box explanations can be more helpful.

Various explanation methods have been developed for computer vision applications (Bach et al., 2015; Fong & Vedaldi, 2017; Montavon, Lapuschkin, Binder, Samek, & Müller, 2017; Nguyen, Dosovitskiy, Yosinski, Brox, & Clune, 2016; Zintgraf, Cohen, Adel, & Welling, 2017). However, most of these methods focus on white-box explanation, i.e. they need to have access to the ML model's internals. So far, few studies have addressed black-box explanation of DL models for image processing tasks. Randomized Input Sampling for Explanation (RISE) (Petsiuk, Das, & Saenko, 2018) estimates a saliency map through probing the object classification model using randomized masking of the input image. It estimates importance scores for pixels of the input image by computing the difference between class probabilities before and after masking the image. Detector Randomized Input Sampling for Explanation (D-RISE) (Petsiuk et al., 2021) adopts the image masking strategy introduced by RISE and provides an attribution method for explaining object detection models. However, a main challenge with RISE and D-RISE is that they need probability scores over classes and an objectness score for every bounding box to estimate the saliency map. Therefore, they may not be useful when the user only has access to bounding box coordinates detected by the model. Another challenge is equal importance assignment to both relevant and irrelevant pixels, which is caused by masks generated in a random manner. This may cause some pixels to be masked more often than other pixels, resulting in a saliency map in which some elements have higher scores because they appeared in more masks. Moreover, a random mask may involve relevant and irrelevant pixels to a detected object. In this case, the same importance is assigned to both the relevant and irrelevant pixels, whereas only masking the relevant pixels has effect on the model's output. As a result, the irrelevant pixels appear as noise in the final saliency map.

In this paper, we address the above challenges by proposing a new explanation method named **Black-box Object Detection Explanation by Masking (BODEM)**. This explanation method is model-agnostic; it can be used to generate explanations for every object detection system regardless of the underlying ML model. Moreover, it does not need to have access to class probabilities or objectness scores. This property makes BODEM suitable for black-box explanation scenarios where we only have access to bounding boxes predicted by the detection model. Our explanation method consists of three main stages, i.e. hierarchical random mask generation, model inquiry, and saliency estimation. In the mask generation phase, coarse-grained masks are generated in higher levels to identify the most salient regions to an object within the input image. Moreover, fine-grained masks are used in lower levels to refine the saliency estimation within the important regions. In the model inquiry step, the detection model is probed with the masked images to examine how its output is changed when some input information is missing. Finally, based on how the model’s output differs from the original output after masking the input, the explanation method computes a saliency map in which the importance of pixels is estimated for every object detected by the object detector. The process of masking, inquiry, and saliency estimation repeats in several iterations, starting from higher levels of the masking hierarchy to lower levels. The final saliency map is used to visualize a heatmap that shows the importance of areas within the image to particular predictions.

Generation of Saliency Maps based on Hierarchical Masking (GSM-HM) (Yan, Li, Zhan, Sun, & Zhu, 2022) is a method of generating saliency maps for object detection models, which also adopts a hierarchical masking strategy. However, the saliency estimation of GSM-HM uses objectness scores, which may not be available in black-box testing and explainability scenarios. On the other hand, our BODEM explainer only requires object coordinates, making it suitable for generating black-box explanations. Moreover, the mechanism of incorporating saliency values from lower levels of the masking hierarchy is different between GSM-HM and our BODEM explainer.

We conducted extensive experiments on three object detection tasks, i.e. user interface control detection, airplane detection, and vehicle detection, using three popular object detection DL models, i.e. YOLO (Redmon et al., 2016), R-CNN (Girshick et al., 2014), and SSD (Wei Liu et al., 2016). We used three quantitative measures to assess the accuracy and stability of explanations. The experimental results showed that our BODEM explanatory outperforms D-RISE with respects to all the three metrics. The results demonstrated that BODEM can be effectively and reliably used to produce explanations that reveal how important different parts of an image are to a particular detection. Investigating the explanations generated by BODEM, we

show that the behaviour of the detection models can be explained, which can help users understand the behaviour of object detectors. Using the explanations generated by BODEM, we reveal some vulnerabilities of the object detectors for particular types of objects.

## 2. Model-agnostic explanation method

In this section, we give a detailed description of the BODEM explanation method. As already explained, BODEM consists of three main stages, i.e. 1) mask generation, 2) model inquiry, and 3) saliency estimation. **Figure 1** illustrates the overall architecture of the explanation method. In the next subsections, we describe these three phases in detail.

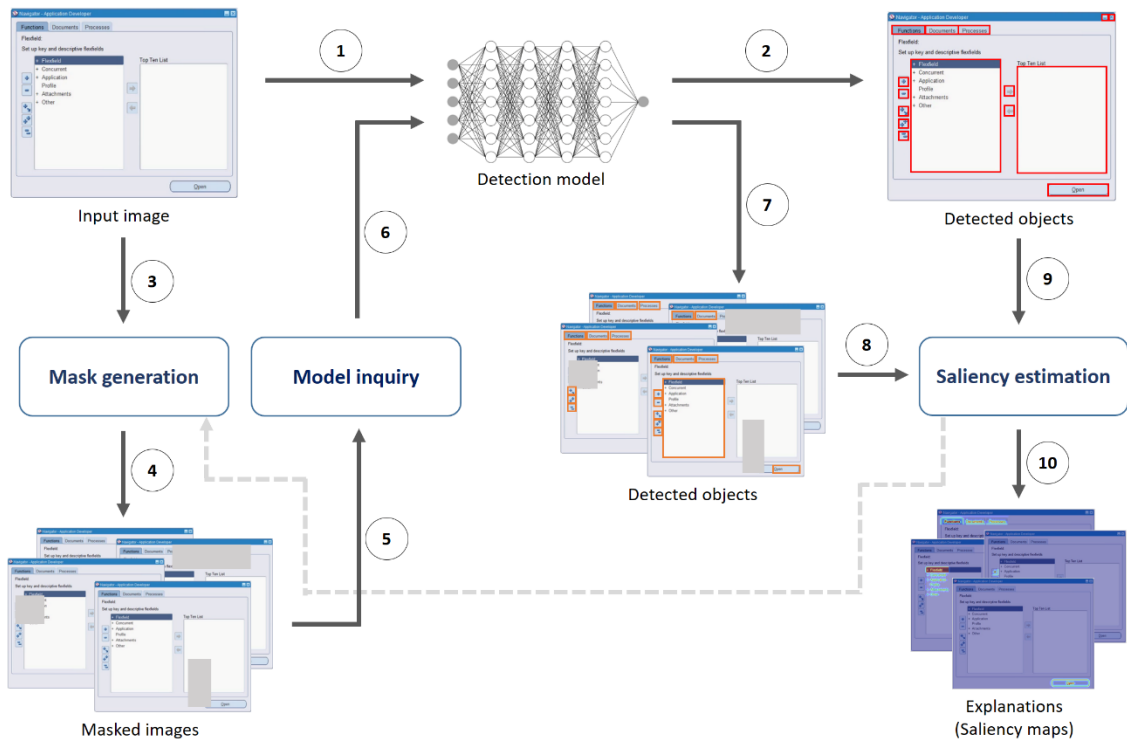


**Figure 1.** The overall architecture of BODEM explanation method. Final explanations are generated through several steps: 1) the input image is fed into the detection ML model, 2) the detection model predicts bounding boxes that specifies the detected objects, 3) the mask generation module receives the input image, 4) it then generates the masked images through a hierarchical masking process, 5) the model inquiry module receives the masked images, 6) it then passes the masked images to the detection model, 7) new predictions are generated for the masked images by the detection model, 8) new bounding boxes are given to the saliency estimation module, 9) the original bounding boxes detected by the ML models are also received by the saliency estimation module, and 10) the final explanations are generated as heatmaps through estimating the saliency of pixels. There is also a connection between the saliency estimation and mask generation modules to control the random mask generation based on the saliency values.

**Problem formulation:** Let  $I$  be an input image with the size of  $W \times H$ . Given an object detector  $f(I) \rightarrow O$ , such that  $O = \{o_1, o_2, \dots, o_N\}$  is a set of objects detected by  $f$ , and every object  $o_n = (x_1, y_1, x_2, y_2)$  is represented as coordinates in a two-dimensional space, the goal is to generate a saliency map  $SM_n$ , for every detected object. The saliency map has a size of  $W \times H$  and contains values that represent the importance of pixels within the input image to the object detected by the target detection model. Our explanation model solves this problem in a black-box manner; it does not need to have access to the architecture, loss function, gradients, weights, or output probabilities of the detection model. Furthermore, it does not require class probabilities and objectness scores for every bounding box detected by the object detector. A main part of our explanation method is a random mask generation technique in combination with a hierarchical masking algorithm, which starts from coarse-grained masks to identify the most salient regions of the image, and continues with fine-grained masks to refine the final explanation and generate a saliency map with smoother salient regions. At each level of the masking hierarchy, only those regions that obtained a non-zero saliency value in the previous level are considered for further refinement. In this way, we incorporate controlled randomness into the mask generation process, leading to less noise in the final saliency map.

## 2.1. Mask generation

As we already discussed in Section 1, a common strategy for black-box explanation of image processing models is to mask different parts of the input image and investigate how the model's output changes when it is fed with the masked images. RISE (Petsiuk et al., 2018) and D-RISE (Petsiuk et al., 2021) adopted random masking strategies, however, random masking has its own shortcomings. The main challenge is that relevant and irrelevant pixels to a particular prediction may be masked at the same time by a random mask. In this case, only the relevant pixels have effect on the model's output, whereas the irrelevant pixels also get importance scores as high as those of the relevant ones. Therefore, those irrelevant pixels will appear as noise in the saliency map.

In order to address this challenge, we propose a masking technique that combines random and hierarchical masking strategies. In the early levels of masking, the explanation method obtains knowledge about those regions of the image that are more salient. This knowledge is then utilized for controlling the mask generation process and continuously refining the saliency map in the later levels.

Given the input image  $I$  and a detected object  $o_n = (x_1, y_1, x_2, y_2)$ , the explanation method starts in the level  $l=1$  by dividing  $I$  into a set of blocks  $B = \{b_1, b_2, \dots, b_p\}$  with a size of  $K \times K$  pixels.

Then, a set of masks  $M=\{m_1, m_2, \dots, m_Q\}$  is generated by selecting blocks from  $B$  and setting the pixel values within those blocks to zero. A block  $b_p$  is a part of mask  $m_q$  and its pixel values must be set to zero if  $m_q(b_p)=1$ . The block  $b_p$  is not masked by  $m_q$  and its pixel values remain unchanged if  $m_q(b_p)=0$ . The mask generation phase in every level is controlled using information obtained from the saliency estimation in the previous level.

First, a set of candidate seed blocks  $CS$  is created and all blocks that obtained a non-zero saliency value in the previous level are added to this set. The first level is an exception because there is no prior information about the saliency of blocks in this level. Therefore, all the blocks in the image are added to  $CS$  in this level. A mask is generated by randomly selecting a seed block from  $CS$  and masking it along with 50 percent of blocks among the neighbors whose distance to the seed block is not larger than  $l$  blocks. The probability of selecting a candidate block as the seed is weighted on its saliency value inherited from the previous level. But those 50 percent of neighboring blocks are selected randomly with equal weights. The fact that salient pixels for an object in the image are naturally appear in the form of a set of continuous regions with various sizes is the rationale behind the idea of selecting blocks in the same neighborhood for generating a mask. At  $l=1$ , all candidate blocks have the same probability of being selected as the seed for generating a mask.

When a block is selected as the seed, it is removed from  $CS$ . The process of selecting a seed and neighboring blocks for generating masks continues until some termination conditions are met. At  $l=1$ , since blocks are bigger and the size of  $CS$  is relatively small, the mask generation process terminates when  $CS$  becomes empty. At levels greater than one, the mask generation continues until 1) all the blocks that inherit a non-zero saliency value from the previous level appear at least once in a mask in the current level, or 2)  $CS$  becomes empty. Since it is likely that all the blocks with a non-zero saliency from the previous level can be included at least once in a mask before the set  $CS$  becomes empty in the current level, the first condition prevents the number of generated masks from becoming very large.

In the next level, the width and height of blocks are divided by two and the size of blocks decreases. For example, in  $l=2$ , every block has a size of  $\frac{K}{2} \times \frac{K}{2}$ . Figure 2 shows examples of blocks and their neighbors with a distance of  $l$  blocks in levels one and two. Seed blocks and neighbor blocks are shown using black and gray colors, respectively. In Figure 1 (a), the level is one, hence, blocks whose distance to the seed block is one block are considered as neighbors and 50 percent of them, i.e. four blocks, are randomly chosen to form a mask. In Figure 1 (b), the level is two, therefore, blocks whose distance to the seed block is two blocks are considered as neighbors and 50 percent of them, i.e. 12 blocks, are randomly chosen to build a mask. As can be

seen, the size of blocks decreases from level  $l$  to  $l+1$ . The area from which blocks are selected and masked becomes smaller in the next level, as represented by red and blue dotted rectangles in Figure 2. In fact, the number of masked blocks increases, the size of blocks decreases, and the masked area becomes smaller as the level goes up.

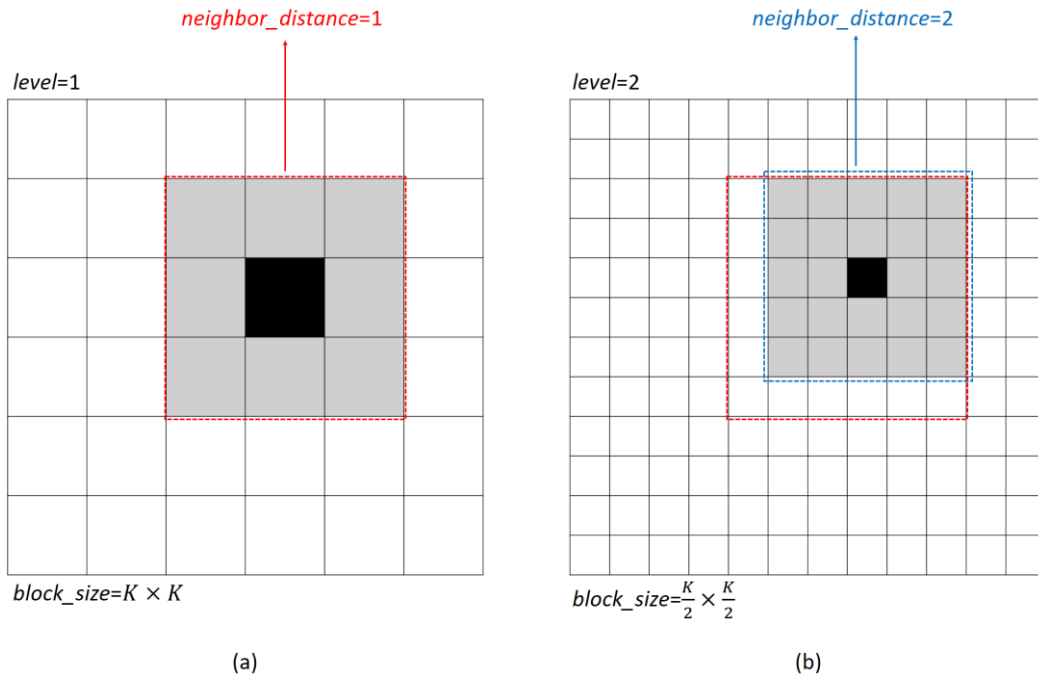


**Figure 2.** Examples of seed blocks and their neighbor blocks in two different levels of the mask generation step. Seed and neighbor blocks are colored by black and gray, respectively.

Algorithm 1 gives the pseudo code of the procedure for mask generation at level  $l$  in our BODEM explanation method. First, the new block size is computed by dividing the block width and height by two, and the image pixels are divided into blocks (lines 3-8). Then, those blocks that obtained non-zero saliency in the previous level are added to the set of candidate seeds (lines 9-14). Then, the process of mask generation proceeds with seed block selection, neighbour selection, and adding them to the list of generated masks (line 15-19). The selected seed is removed from the list of candidate blocks, the termination conditions are checked, and if the conditions are met, the mask generation procedure finishes at level  $l$  and the list of masks are returned (20-25).

**Algorithm 1.** The mask generation procedure at level  $l$  used by our BODEM explanation method.

---

- 1: **Inputs:** input image  $I$ , detected object  $O_n$  within  $I$ , saliency map  $SM_n$ , block size in previous level  $BS^{l-1}=K \times K$
  - 2: **Output:** set of masks  $M^l$  at level  $l$
  - 3: **if**  $l=1$  **then**
  - 4:    $BS^l = K \times K$  (there is no previous level at level one)
  - 5: **else if**  $l>1$  **then**
  - 6:    $BS^l = \frac{BS^{l-1}}{2} = \frac{K}{2} \times \frac{K}{2}$
  - 7: **end if**
  - 8: Divide pixels within  $I$  into a set of blocks  $B^l = \{b_1, b_2, \dots, b_P\}$  with block size  $BS^l$
  - 9: Create a set of candidate seeds  $CS = \emptyset$
  - 10: Create a set of masks  $M^l = \emptyset$
  - 11: **for** every block  $b_p \in B^l$  **do**:
  - 12:   **if**  $l=1$  **then** add  $b_p$  to  $CS$
  - 13:   **else if**  $l>1$  and  $SM_n^{l-1}[b_p]$  has any non-zero values **then** add  $b_p$  to  $CS$
  - 14: **end for**
  - 15: **while** termination conditions are not met **do**:
  - 16:   Randomly select a block  $b_p$  from  $CS$  as a seed with a probability weighted on saliency  $SM_n^{l-1}[b_p]$
  - 17:   Randomly select 50 percent of neighbors of  $b_p$  whose distance with  $b_p$  is not larger than  $l$  blocks
  - 18:   Create a mask  $m_q$  where block  $b_p$  and the selected neighboring blocks are masked
  - 19:   Add  $m_q$  to  $M^l$
  - 20:   Remove  $b_p$  from  $CS$
  - 21:   Check termination conditions:
  - 22:     **if**  $l=1$  **then** termination condition is:  $CS$  becomes empty
  - 23:     **if**  $l>1$  **then** termination conditions are:  $CS$  becomes empty or every block  $b_p \in B^l$  with  $SM_n^{l-1}[b_p] > 0$  appears at least in one mask
  - 24: **end while**
  - 25: **return**  $M^l$
-

## 2.2. Model inquiry

The model inquiry module acts as an intermediary between the explanation model and the object detection model. It receives a masked image, sends the image to the object detection model, receives new bounding boxes detected by the object detector, and passes them to the next step, i.e. the saliency estimation module. The inquiry module is model-agnostic and has no information about the neural network architecture, loss function, activation functions, connection weights, and hyperparameters of the underlying ML model. It sends requests to the detection model and receives bounding box coordinates predicted by the model. Therefore, the explanation method can be used to explain any object detection systems, regardless of the underlying ML model, making it suitable for black-box software testing scenarios.

## 2.3. Saliency estimation

The saliency estimation module receives the original object coordinates  $o_n=(x_l, y_l, x_2, y_2)$  generated by the object detection model  $f$  and new object coordinates  $o'_n=(x'_l, y'_l, x'_2, y'_2)$  predicted for the masked image. Its main task is to estimate the importance of pixels within the input image by measuring the difference between the original and new predictions. It then updates the saliency map  $SM_n$  that represents the importance of different parts of the image to the object  $o_n$ . The saliency map  $SM_n$  is initially filled with zero values. It is worth to note that if several objects are detected within the masked image, the nearest one to  $o_n$  is considered as  $o'_n$ .

At level  $l$ , given the original object coordinates  $o_n=(x_l, y_l, x_2, y_2)$  detected within the image  $I$ , a mask  $m_q$  applied to the image, the new object coordinates  $o'_n=(x'_l, y'_l, x'_2, y'_2)$  detected within the masked image  $I'$ , and a saliency map  $SM_n$ , the saliency estimation module first computes the similarity between  $o_n$  and  $o'_n$  using Intersection Over Union (IOU), as follows:

$$Similarity(o_n, o'_n) = IOU(o_n, o'_n) = \frac{|o_n \cap o'_n|}{|o_n \cup o'_n|} \quad (1)$$

The computed similarity falls in the range  $[0, 1]$ . If the saliency estimation module has access to the objectness score or class probabilities, they can also contribute to the similarity measure in Equation (1). In this paper, we address the extreme black-box scenario, i.e. having access to only object coordinates, but other object detection outputs can be simply included in Equation (1) to measure the similarity between two objects.

A similarity value close to one refers to little or no difference between  $o_n$  and  $o'_n$ . Therefore, those blocks that were masked within  $I'$  had little or no importance to the target object. On the other hand, A similarity value close to zero refers to the high importance of the masked blocks to the target object, because the absence of those pixels led the object detector to predict a wrong

bounding box. Given the similarity value, an importance score  $IS$  is computed for every block  $b_p$  that was covered by the mask  $m_q$ , as follows:

$$IS(b_p) = 1 - \text{Similarity}(o_n, o'_n) \quad (2)$$

After computing an importance score for every block that was masked in an image at level  $l$ , an overall importance score  $OIS$  is computed for every block  $b_p$  by taking the average of all importance scores over all images where  $b_p$  was masked at this level, as follows:

$$OIS(b_p) = \frac{\sum_{m_q \in M^l | m_q(b_p)=1} IS(b_p)}{\sum_{m_q \in M^l} m_q(b_p) = 1} \quad (3)$$

where  $M^l$  is the set of all masks at level  $l$ . In Equation (3), the numerator sums up all the importance scores of the block  $b_p$  for every mask where  $b_p$  was masked at level  $l$ , and the denominator counts in how many masks the block  $b_p$  was masked at level  $l$ . In fact, the larger the  $OIS(b_p)$ , the more the importance of block  $b_p$  for detecting the target object.

Now that an overall importance score has been computed for every block, the saliency map  $SM_n$  is updated to represent the saliency of blocks at the current level. It is worth noting that only those blocks whose value in the saliency map was non-zero at level  $l-1$  participate in the saliency estimation phase at level  $l$ . If a block was assigned zero as the saliency value at level  $l-1$ , its saliency value will be zero at level  $l$  as well. Moreover, if a block obtained a non-zero saliency value at level  $l-1$  but receives an overall importance score of zero at level  $l$ , it inherits the saliency value from the previous level, however, the saliency value becomes smaller to penalize the block for not being salient in the current level.

The new saliency value of a block is computed by combining its saliency from the previous level with the overall importance score in the current level, as follows:

$$SM_n^l[b_p] = \begin{cases} (\alpha)SM_n^{l-1}[b_p] + (1 - \alpha)OIS(b_p), & \exists m_q \in M^l | m_q(b_p) = 1 \text{ and } OIS(b_p) \neq 0 \\ (\beta)SM_n^{l-1}[b_p], & \text{otherwise} \end{cases} \quad (4)$$

where  $\alpha$  is a hyperparameter that controls how much influence the block  $b_p$  must get from its saliency value in the previous level. The higher the value of  $\alpha$ , the more influence the saliency value at level  $l-1$  has on the saliency of the block at level  $l$ . Another hyperparameter in this equation is  $\beta$  that controls how much the block  $b_p$  must be penalized if it does not obtain an overall importance score higher than zero in the current level. The lower the value of  $\beta$ , the more the block  $b_p$  is penalized by inheriting less saliency value from the previous level. Both the hyperparameters  $\alpha$  and  $\beta$  have a value in the range  $[0, 1]$ .

The process of mask generation, model inquiry, and saliency estimation continues until the explanation method finishes the process at the last level. The saliency map obtained at the last

level contains the most detailed saliency values resulted from being refined through several iterations of coarse-grained and fine-grained masking and saliency estimation. Therefore, the saliency map estimated at the last level is used by our BODEM method as the final explanation for the target object.

Algorithm 2 gives the pseudo code of the procedure for saliency estimation at level  $l$  in our BODEM explanation method. First, the similarity between the objects in the original and masked images is computed, and an importance score is subsequently estimated for blocks that were masked (lines 3-10). Then, an overall importance score is computed for the masked blocks, the saliency map is updated for those blocks whose saliency value was larger than zero in the previous level, and the saliency map is returned (lines 11-17).

**Algorithm 2.** The saliency estimation procedure at level  $l$  used by our BODEM explanation method.

---

```

1: Inputs: detected object  $O_n$  within image  $I$ , a set of masks  $M^l = \{m_1, m_2, \dots, m_Q\}$  applied to  $I$ ,
   set of detected objects  $O'_n = \{O'_n{}^1, O'_n{}^2, \dots, O'_n{}^Q\}$  within masked images  $I'_1, I'_2, \dots, I'_q$  such that
    $O'_n{}^q$  was detected within  $I'_q$ , set of blocks  $B^l = \{b_1, b_2, \dots, b_P\}$  at level  $l$ , saliency map  $SM_n^{l-1}$ 
   from previous level
2: Outputs: saliency map  $SM_n^l$  after updating in current level
3: for every object  $O'_n{}^q$  such that it was detected in image  $I'_q$  masked by  $m_q$  do:
4:   Compute  $Similarity(O_n, O'_n{}^q)$  using Equation (1)
5:   for every  $b_p \in B^l$  do:
6:     if  $m_q(b_p) = 1$  then:
7:       Compute and store an importance score  $IS(b_p)$  using Equation (2)
8:     end if
9:   end for
10: end for
11: for every  $b_p \in B^l$  do:
12:   Compute an overall importance score  $OIS(b_p)$  using equation (3) and importance scores
   computed in line 7
13:   if  $SM_n^{l-1}[b_p] > 0$  then:
14:     Update  $SM_n^l[b_p]$  using Equation (4)
15:   end if
16: end for
17: return  $SM_n^l$ 

```

---

Figure 3 shows an input image and a button user interface control detected within the input image, along with the saliency maps generated by our BODEM explanation method at different levels. As can be seen, at the coarse-grained levels, e.g.  $l=1$  and  $l=2$ , where blocks are larger, the salient regions of the image are identified by the explanation method, however, the saliency map is not accurate enough and important regions have no smooth boundaries. On the other hand, at the fine-grained levels, e.g.  $l=6$ , where blocks are smaller, the salient regions are refined. Consequently, the final saliency map can represent the salient regions, objects, lines, etc. more accurately, with smoother boundaries.

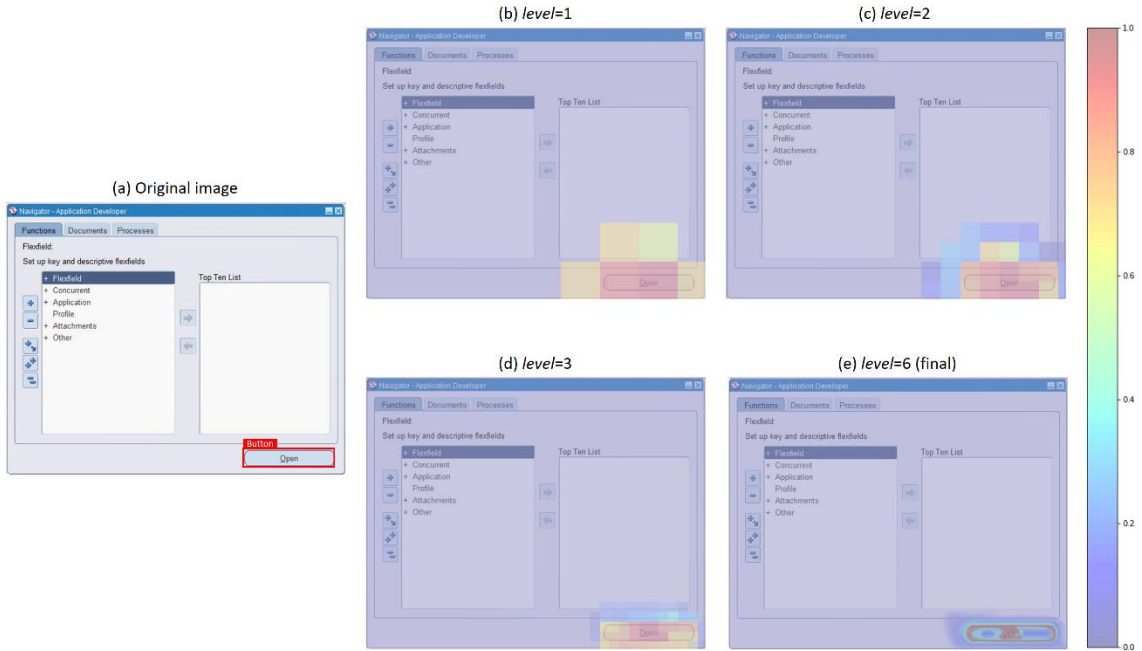


**Figure 3.** An input image and saliency maps generated by our BODEM explanation method at different levels for a detected button user interface control. In this example, the block size is  $128 \times 128$ ,  $64 \times 64$ ,  $32 \times 32$ ,  $16 \times 16$ ,  $8 \times 8$ , and  $4 \times 4$  pixels at level 1, 2, 3, 4, 5, and 6, respectively.

### 3. Experimental results

In this section, we first describe the datasets, evaluation metrics, and object detection models that we utilized in our experiments. We then present the object detection test results, as well as explanations produced by our BODEM explainer. Moreover, we give examples where explanations can help to analyze which parts of objects are more important to the object detectors. In the experiments presented in this section, we used six levels of masks with the following sizes in the BODEM explanation method:  $128 \times 128$ ,  $64 \times 64$ ,  $32 \times 32$ ,  $16 \times 16$ ,  $8 \times 8$ , and  $4 \times 4$ . The experimental details, data, and source codes can be accessed at <https://github.com/mmoradi-iut/BODEM>.

### 3.1. Datasets

**User interface control detection:** Our main focus for developing the explanation method was on the user interface control detection task for automated software testing. This is a private dataset, which contains 16,155 images annotated for detection and classification of 18 types of user interface controls. The images are digital screenshots taken from desktop, Software as a Service (SaaS), and mobile applications. We split the dataset into a train and development set containing 14,155 images, and a test set containing 2,000 images.

**Airplane detection**<sup>1</sup>: This public dataset contains 733 aerial images annotated for detecting airplanes. We split the dataset into a train and development set with 650 images, and a test set with 83 images. We chose to use this small dataset in order to investigate how the BODEM explanation method can be effective in scenarios where there are not many images to train an object detection model.

**Vehicle detection:** Common Objects in Context (COCO) dataset (Lin et al., 2014) is a large dataset of more than 160,000 images annotated for object detection and classification of 80 object categories. We created a subset of 8,000 images from COCO for our vehicle detection task by randomly choosing 2,000 images from each one of the categories “CAR”, “BUS”, “TRUCK”, and “MOTORCYCLE”. The train and development set of this new dataset has 7,000 images. The test set contains 1,000 images.

### 3.2. Evaluation metrics

We used three different evaluation metrics to objectively evaluate the effectiveness of our explanation method against D-RISE. The evaluation metrics are as follows:

**Deletion:** Pixels of the original image are deleted one by one in descending order of their saliency value, and the difference between the detection results of the original image and the image with deleted pixels is computed as the IOU between the objects detected within the images. We use the mean detection difference Area Under the Curve (AUC) across all the images in the test set as the final deletion measure to evaluate the explanation methods.

**Insertion:** First, a version of the original image is created where pixels of the saliency area are deleted. Then, pixels are filled one by one into the image in descending order of their saliency value, and the difference between the detection results of the original image and the image filled with salient pixels is computed as the IOU between the objects detected within the images. We

---

<sup>1</sup> <https://www.kaggle.com/datasets/airbusgeo/airbus-aircrafts-sample-dataset>

use the mean insertion difference AUC across all the images in the test set as the final insertion measure to evaluate the explanation methods.

**Convergence:** This metric estimates the ability of methods in generating stable saliency maps for the same object. We measure the convergence by calculating the difference between three saliency maps resulted from running the explanation method three times (with the same experimental settings) on the same input image. The Euclidean distance is used to calculate the difference between saliency maps, as follows:

$$Convergence = \frac{\|SM_1 - SM_2\| + \|SM_1 - SM_3\| + \|SM_2 - SM_3\|}{3} \quad (5)$$

where  $\|SM_1 - SM_2\|$  denotes the Euclidean distance between two saliency maps  $SM_1$  and  $SM_2$ . A smaller Euclidean distance refers to a better convergence, which subsequently means more stable saliency maps generated by the explanation method.

### 3.3. Object detection models

Object detection models can be generally divided into one-stage and two-stage methods. Two-stage detectors break down the problem into two steps, i.e. 1) detecting region proposals, which possibly contain an instance of an object of interest, and 2) classifying those regions with respect to the probability of an object appearing within a region. On the other hand, one-stage detectors utilize end-to-end neural networks to predict bounding boxes and class probabilities of detected objects all at once. We used both one-stage and two-stage object detection models in our experiments.

**YOLO** (Redmon et al., 2016): It is a one-stage object detection algorithm that divides the input image into  $N$  grids with equal size, and then detects and localizes objects within each grid. In order to handle overlapping bounding boxes detected within different grids, YOLO utilizes Non-Maximal Suppression (NMS), which is a technique to filter grids and select regions with the highest probability of containing an object of interest. Due to its one-stage detection strategy, YOLO can perform much faster than popular two-stage detectors such as R-CNN and Fast R-CNN. That is why it is widely used for real-time object detection. Inspired by the GoogleNet architecture, YOLO composes of 24 convolutional layers followed by two fully-connected layers. We used YOLO-v5 in our experiments, and trained it on the user interface control detection dataset.

**R-CNN** (Girshick et al., 2014): This object detector uses selective search to extract region proposals, which are then fed to a CNN that classifies the regions as they contain a target object or not. As the backbone of this object detector, we used a VGG-16 model, which has a CNN with

16 convolutional layers and 134 million parameters. This CNN was already pretrained on more than one million images from the ImageNet dataset<sup>2</sup>. One flatten layer, two fully-connected dense layers, and a softmax layer for the final classification were added to the backbone model. We froze all layers of the backbone except the last three convolutional layers. We then fine-tuned the remaining layers and our custom layers on the airplane detection dataset.

**SSD (Wei Liu et al., 2016):** It is another one-stage detection model that is composed of two components, i.e. a backbone model, and SSD head. A pretrained model is usually utilized as the backbone to serve as a feature extractor. SSD head is usually formed by several convolutional layers on top of the backbone. These additional layers are specifically trained for the object detection task at hand. In our experiments, we used a variant of SSD that has ResNet-101, which were pretrained on ImageNet, with around 44 million parameters as the backbone. Six more convolutional layers were added on top of the backbone to form the SSD head and train it for our object detection task. We fine-tuned the SSD model on the vehicle detection dataset.

### 3.4. Hyperparameter tuning

As we explained in Section 2.3, there are two hyperparameters that control how the saliency map is updated at level  $l$  using the saliency values estimated at level  $l-1$ . The hyperparameter  $\alpha$  controls how much saliency a block inherits from its saliency value from the previous level. Smaller values of this hyperparameter give a higher weight to the saliency score estimated at the current level, while larger values assign a higher weight to the saliency value estimated at the previous level. The hyperparameter  $\beta$  controls how much a block is penalized if it gets a zero saliency value at the current level. Smaller values of this hyperparameter give larger penalties by letting the block inherit only a small proportion of the saliency value it had at the previous level. In this way, if  $\beta$  has a small value, the saliency value of a block shrinks by a large proportion at the next levels if it gets a zero saliency score at the current level.

We conducted a set of hyperparameter tuning experiments on the training sets to find optimal values for  $\alpha$  and  $\beta$ , with respect to the accuracy of the explanations and the visual quality of the saliency maps. The results were to a high extent similar across all the three datasets. We observed the highest performance scores and visual quality of saliency maps when  $\alpha=0.3$  and  $\beta=0.2$ . Therefore we used these hyperparameter values in the subsequent experiments on the test sets.

---

<sup>2</sup> <https://www.image-net.org/>

### 3.5. User interface control detection

We trained the YOLO detection model on the user interface control detection dataset. **Table 1** presents the performance scores obtained by the YOLO object detection model on the respective test set. Although these scores are not relevant to the experiments we performed to evaluate the effectiveness of the explanation methods, we present them in the paper just to give the reader an idea how well the object detection model performed on this task.

**Table 1.** Performance scores obtained by the YOLO object detection model on the user interface control detection test set.

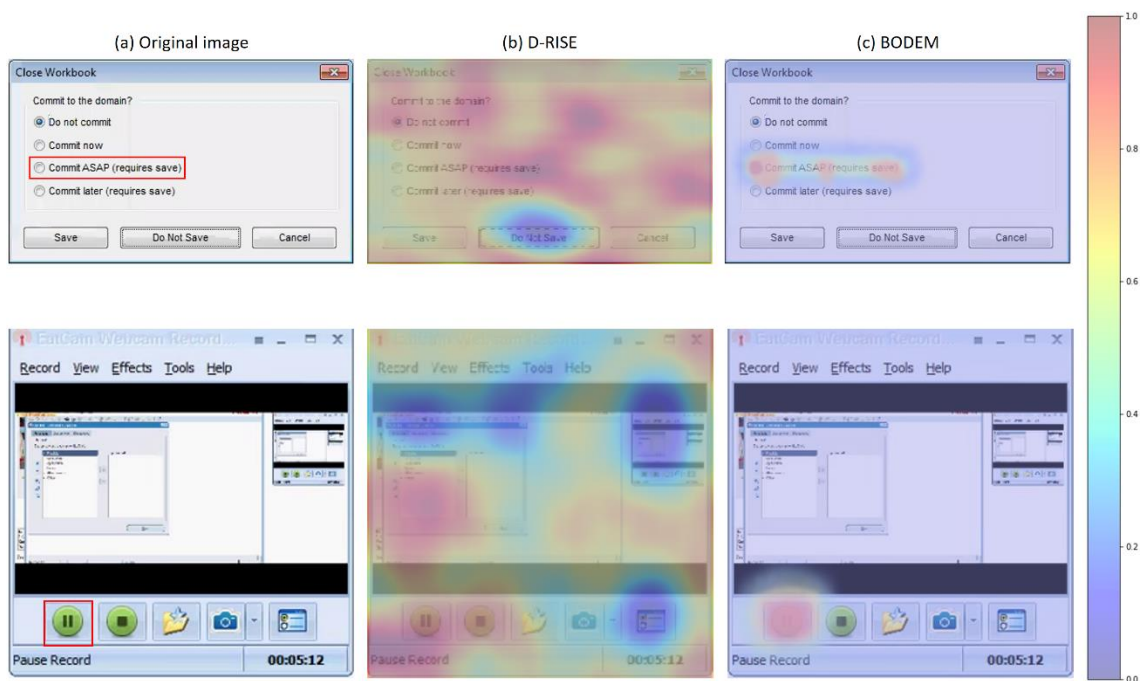
| Class              | Precision | Recall | mAP@.5 | mAP@.95 |
|--------------------|-----------|--------|--------|---------|
| ALL                | 0.799     | 0.752  | 0.75   | 0.588   |
| ICON               | 0.931     | 0.88   | 0.883  | 0.611   |
| DROPDOWN           | 0.886     | 0.907  | 0.904  | 0.748   |
| BUTTON             | 0.893     | 0.861  | 0.886  | 0.773   |
| MENU               | 0.836     | 0.512  | 0.523  | 0.4     |
| INPUT              | 0.913     | 0.748  | 0.758  | 0.663   |
| LIST               | 0.674     | 0.709  | 0.636  | 0.481   |
| TABBAR             | 0.905     | 0.582  | 0.645  | 0.562   |
| TABLE              | 0.815     | 0.862  | 0.825  | 0.747   |
| RADIO_SELECTED     | 0.916     | 0.916  | 0.946  | 0.68    |
| RADIO_UNSELECTED   | 0.856     | 0.957  | 0.918  | 0.688   |
| CHECKBOX_UNCHECKED | 0.891     | 0.94   | 0.925  | 0.654   |
| CHECKBOX_CHECKED   | 0.905     | 0.887  | 0.904  | 0.591   |
| TREE               | 0.77      | 0.769  | 0.749  | 0.63    |

Table 2 reports the performance evaluation scores obtained by our BODEM explanation method and D-RISE on the objects detected by the YOLO model on the user interface control detection dataset. As can be seen, BODEM obtained a lower mean deletion AUC than D-RISE. This demonstrates that BODEM performs more accurate than D-RISE in detecting the salient regions within the images, as deleting salient pixels detected by BODEM results in a more rapid decrease in the detection accuracy in comparison to D-RISE. Moreover, a higher mean insertion AUC is reported for BODEM. It again refers to the superior ability of BODEM in comparison to D-RISE in detecting the most salient image areas, as inserting the salient pixels identified by BODEM into the images led to a quicker increase in the detection accuracy. Our BODEM explainer also obtained a better mean convergence, demonstrating its ability to generate more

stable saliency maps. The hierarchical masking strategy has the most contribution to the stability of saliency maps by controlling the randomness and limiting random masks to the most salient regions instead of the whole image.

**Table 2.** The results of performance evaluation experiments obtained by the BODEM and D-RISE explanation methods on the objects detected by the YOLO model on the user interface control detection dataset. The best result in each column is shown in underlined face.

| Explanation method | Mean deletion AUC | Mean insertion AUC | Mean convergence |
|--------------------|-------------------|--------------------|------------------|
| D-RISE             | 0.113             | 0.612              | 18.406           |
| BODEM              | <u>0.058</u>      | <u>0.875</u>       | <u>6.051</u>     |



**Figure 4.** User interface controls detected by the YOLO model within two images, and saliency maps generated by our BODEM explanation method and D-RISE for the detected objects.

Figure 4 shows examples of user interface controls detected by the YOLO object detector, and saliency maps generated by our BODEM explainer and D-RISE. As can be seen, the saliency maps generated by D-RISE somehow identified the salient regions to the detected objects, however, it identified some irrelevant regions as salient as well. On the other hand, our BODEM explainer managed to identify the most salient regions more accurately than D-RISE, with significantly less noise within the saliency maps.

Observing many explanations produced by the BODEM explainer helped us find some patterns that can be useful for inspection and validation of the detection model: 1) lines that specify the borders of controls are very important to the model, 2) icons within BUTTON controls

have high impacts on detecting correct boundaries, 3) correct detection of small controls, such as CHECKBOX, is highly dependent on the neighboring areas within the image, such that perturbing small parts of neighboring area can mislead the object detector, 4) texts within controls such as MENU have large effects on the correct predictions, 5) detecting those BUTTON controls that are close to other controls is also influenced by the borders of neighboring controls, in addition to the control’s borders, and other similar patterns. These observations convey that explanations generated by BODEM can effectively help us understand the behavior of the detection model.

### 3.6. Airplane detection

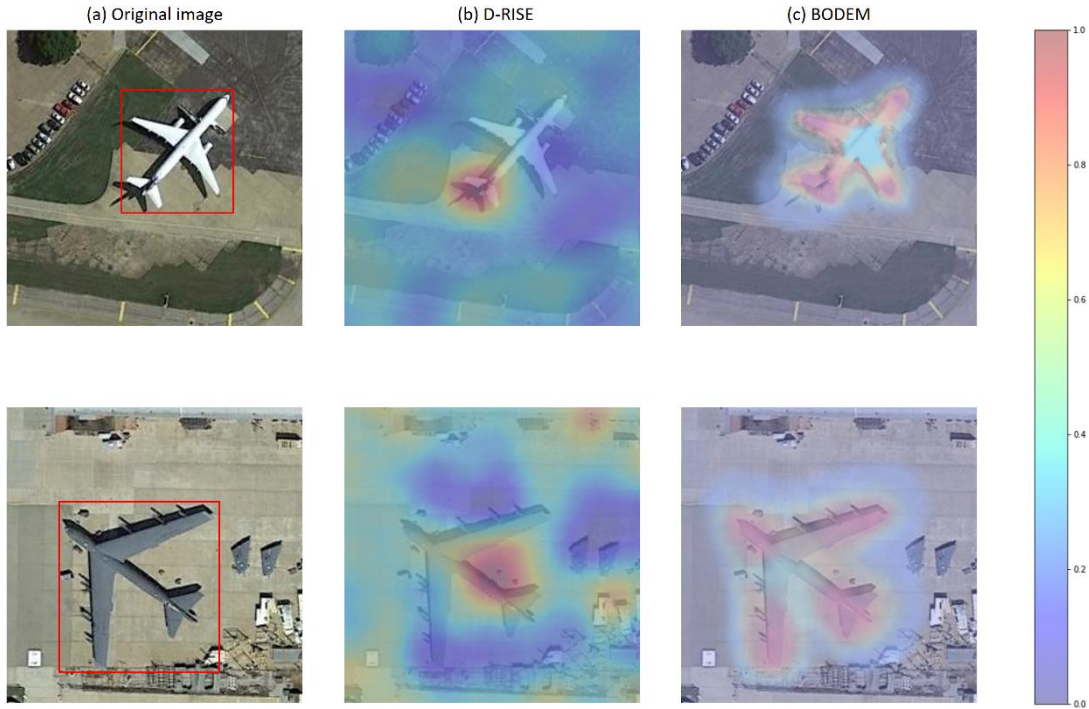
We trained the R-CNN detection model on the airplane detection dataset. The model achieved an accuracy of 87.05% on the test set. We utilized our BODEM explanation method to understand which parts of the objects detected by the detection model are more important and have higher impacts on the model’s decisions.

Table 3 presents the performance evaluation scores obtained by our BODEM explanation method and D-RISE on the objects detected by the R-CNN model on the airplane detection dataset. As the results show, our BODEM explainer outperforms D-RISE with respect to the mean deletion AUC, mean insertion AUC, and mean convergence. This demonstrates the effectiveness of the saliency maps generated by BODEM in identifying the most important regions to the detected objects in the images.

Figure 5 shows examples of airplanes detected by the R-CNN object detector, and saliency maps generated by our BODEM explainer and D-RISE. As can be seen, similar to the user interface control detection dataset, the saliency maps generated by BODEM contain less noise and identify the most important regions more accurately than those generated by D-RISE. As the saliency maps show, the head, wings and tail of the airplanes have more impact than other parts on detecting the airplanes. This is a common pattern in many objects detected by the model, suggesting that the object detector decides about the bounding boxes by paying more attention to the head, wings, and tail of an airplane.

**Table 3.** The results of performance evaluation experiments obtained by the BODEM and D-RISE explanation methods on the objects detected by the R-CNN model on the airplane detection dataset. The best result in each column is shown in underlined face.

| Explanation method | Mean deletion AUC | Mean insertion AUC | Mean convergence |
|--------------------|-------------------|--------------------|------------------|
| D-RISE             | 0.128             | 0.597              | 19.512           |
| BODEM              | <u>0.064</u>      | <u>0.856</u>       | <u>7.133</u>     |



**Figure 5.** Airplanes detected by the R-CNN model within two images, and saliency maps generated by our BODEM explanation method and D-RISE for the detected objects.

### 3.7. Vehicle detection

We trained the SSD detection model on the vehicle detection dataset. **Table 4** presents the performance scores obtained by the SSD object detection model on the respective test set. Although these scores are not relevant to the experiments we performed to evaluate the effectiveness of the explanation methods, we present them in the paper just to give the reader an idea how well the object detection model performed on this task.

**Table 4.** The performance scores obtained by the SSD detection model on the vehicle detection test set.

| Class      | Precision | Recall | mAP@.7 |
|------------|-----------|--------|--------|
| ALL        | 0.813     | 0.780  | 0.765  |
| CAR        | 0.844     | 0.801  | 0.783  |
| BUS        | 0.819     | 0.781  | 0.765  |
| TRUCK      | 0.785     | 0.752  | 0.742  |
| MOTORCYCLE | 0.803     | 0.788  | 0.771  |

Table 5 reports the performance evaluation scores obtained by our BODEM explanation method and D-RISE on the objects detected by the SSD model on the vehicle detection dataset. Similar to the results reported on the other two datasets, BODEM obtained better results than D-RISE regarding all the metrics. This again demonstrates the effectiveness of our explanation method for identifying the most salient regions to the objects across various detection tasks.

Figure 6 shows examples of vehicles detected by the SSD object detector, and saliency maps generated by our BODEM explainer and D-RISE. Similar to the saliency maps generated for the other two tasks, BODEM managed to generate more accurate explanations with less amounts of noise. As the explanations show, the wheels, hood, and boot had higher impacts on detecting the car. The wheels and seat were more important for detecting the motorcycle. Observing several explanations, we found similar patterns in the objects detected by the SSD detection model on the vehicle detection dataset. We also found that the object detector paid more attention to the head and wheels for predicting bounding boxes around buses. Another observation is that the head, wheels, and lower parts of the truck objects had a higher importance to the detection model for this particular class.

**Table 5.** The results of performance evaluation experiments obtained by the BODEM and D-RISE explanation methods on the objects detected by the SSD model on the vehicle detection dataset. The best result in each column is shown in underlined face.

| Explanation method | Mean deletion<br>AUC | Mean insertion<br>AUC | Mean convergence |
|--------------------|----------------------|-----------------------|------------------|
| D-RISE             | 0.137                | 0.605                 | 17.381           |
| BODEM              | <u>0.069</u>         | <u>0.860</u>          | <u>6.420</u>     |

## 4. Conclusion

In this paper, we proposed BODEM, a method for explaining the output of object detection models in a black-box manner. Our explanation method utilizes a hierarchical random masking strategy to identify the most important regions to an object within the input image and estimate a saliency map. We conducted extensive experiments on various object detection models and datasets, using different objective evaluation metrics. The results showed that BODEM can be effectively used to generate visual explanations that reveal which parts of images and objects are more important when an object detector makes a decision. The explanations helped us find useful patterns about the behavior of detection models on different tasks and objects. The explanation method does not need to have access to the underlying ML model’s internals or any other

information about its structure or settings. This makes BODEM a proper choice for explaining and validating the behavior of object detection systems and reveal their vulnerabilities in black-box software testing scenarios. It was already investigated how failure points of natural language processing models can be revealed by injecting small amounts of noise into the input and observing changes in the behavior of the models (Moradi & Samwald, 2021a).



**Figure 6.** Vehicles detected by the SSD model within two images, and saliency maps generated by our BODEM explanation method and D-RISE for the detected objects.

Developing XAI methods for computer vision tasks is crucial for enhancing transparency, trust, and understanding in AI systems. Future research may address the expansion of BODEM to explanation methods for other computer vision tasks such as classification or segmentation. Other future lines of work may include: 1) combining deep learning with symbolic reasoning to provide more interpretable models, 2) integrating human feedback into the learning process to refine and improve the explainability of AI systems, 3) developing methods that can provide explanations using multiple modalities (e.g., text, visualizations, audio) to cater to different user needs and accessibility requirements, 4) for tasks such as video analysis and real-time object detection, developing methods to explain the temporal and spatial dynamics influencing model decisions, 5) researching how explainability techniques can contribute to the robustness and generalization of computer vision models, and 6) Establishing benchmarks and standardized evaluation metrics for explainability in computer vision.

## References

- Adadi, A., & Berrada, M. (2018). Peeking Inside the Black-Box: A Survey on Explainable Artificial Intelligence (XAI). *IEEE Access*, 6, 52138-52160. doi: <https://doi.org/10.1109/ACCESS.2018.2870052>
- Ammann, P., & Offutt, J. (2016). *Introduction to software testing*: Cambridge University Press.
- Bach, S., Binder, A., Montavon, G., Klauschen, F., Müller, K.-R., & Samek, W. (2015). On Pixel-Wise Explanations for Non-Linear Classifier Decisions by Layer-Wise Relevance Propagation. *PLOS ONE*, 10(7), e0130140. doi: <https://doi.org/10.1371/journal.pone.0130140>
- Devlin, J., Chang, M.-W., Lee, K., & Toutanova, K. (2018). Bert: Pre-training of deep bidirectional transformers for language understanding. *arXiv preprint arXiv:1810.04805*.
- Fong, R. C., & Vedaldi, A. (2017). *Interpretable explanations of black boxes by meaningful perturbation*. Paper presented at the Proceedings of the IEEE International Conference on Computer Vision.
- Freitas, A. A. (2014). Comprehensible classification models: a position paper. *SIGKDD Explor. Newsl.*, 15(1), 1–10. doi: 10.1145/2594473.2594475
- Girshick, R. (2015). *Fast r-cnn*. Paper presented at the Proceedings of the IEEE international conference on computer vision.
- Girshick, R., Donahue, J., Darrell, T., & Malik, J. (2014). *Rich feature hierarchies for accurate object detection and semantic segmentation*. Paper presented at the Proceedings of the IEEE conference on computer vision and pattern recognition.
- Gu, J., Wang, Z., Kuen, J., Ma, L., Shahroudy, A., Shuai, B., . . . Chen, T. (2018). Recent advances in convolutional neural networks. *Pattern Recognition*, 77, 354-377. doi: <https://doi.org/10.1016/j.patcog.2017.10.013>
- Guidotti, R., Monreale, A., Ruggieri, S., Turini, F., Giannotti, F., & Pedreschi, D. (2018). A Survey of Methods for Explaining Black Box Models. *ACM Comput. Surv.*, 51(5), 1-42. doi: <https://doi.org/10.1145/3236009>
- He, K., Gkioxari, G., Dollár, P., & Girshick, R. (2017). *Mask r-cnn*. Paper presented at the Proceedings of the IEEE international conference on computer vision.
- Jiao, L., Zhang, F., Liu, F., Yang, S., Li, L., Feng, Z., & Qu, R. (2019). A Survey of Deep Learning-Based Object Detection. *IEEE Access*, 7, 128837-128868. doi: 10.1109/ACCESS.2019.2939201
- Jordan, M. I., & Mitchell, T. M. (2015). Machine learning: Trends, perspectives, and prospects. *Science*, 349(6245), 255-260.
- Khamparia, A., & Singh, K. M. (2019). A systematic review on deep learning architectures and applications. *Expert Systems*, 36(3), e12400. doi: <https://doi.org/10.1111/exsy.12400>
- LeCun, Y., Bengio, Y., & Hinton, G. (2015). Deep learning. *Nature*, 521(7553), 436-444. doi: <https://doi.org/10.1038/nature14539>
- Li, Z., Liu, F., Yang, W., Peng, S., & Zhou, J. (2022). A Survey of Convolutional Neural Networks: Analysis, Applications, and Prospects. *IEEE Transactions on Neural Networks and Learning Systems*, 33(12), 6999-7019. doi: 10.1109/TNNLS.2021.3084827
- Lin, T.-Y., Maire, M., Belongie, S., Hays, J., Perona, P., Ramanan, D., . . . Zitnick, C. L. (2014). *Microsoft COCO: Common Objects in Context*, Cham.
- Liu, W., Anguelov, D., Erhan, D., Szegedy, C., Reed, S., Fu, C.-Y., & Berg, A. C. (2016). *SSD: Single Shot MultiBox Detector*, Cham.
- Liu, W., Wang, Z., Liu, X., Zeng, N., Liu, Y., & Alsaadi, F. E. (2017). A survey of deep neural network architectures and their applications. *Neurocomputing*, 234, 11-26. doi: <https://doi.org/10.1016/j.neucom.2016.12.038>

- Montavon, G., Lapuschkin, S., Binder, A., Samek, W., & Müller, K.-R. (2017). Explaining nonlinear classification decisions with deep Taylor decomposition. *Pattern Recognition*, 65, 211-222. doi: <https://doi.org/10.1016/j.patcog.2016.11.008>
- Moradi, M., & Samwald, M. (2021a). *Evaluating the Robustness of Neural Language Models to Input Perturbations*, Online and Punta Cana, Dominican Republic.
- Moradi, M., & Samwald, M. (2021b). Explaining Black-Box Models for Biomedical Text Classification. *IEEE Journal of Biomedical and Health Informatics*, 25(8), 3112-3120. doi: <https://doi.org/10.1109/JBHI.2021.3056748>
- Moradi, M., & Samwald, M. (2021c). Post-hoc explanation of black-box classifiers using confident itemsets. *Expert Systems with Applications*, 165, 113941. doi: <https://doi.org/10.1016/j.eswa.2020.113941>
- Moradi, M., & Samwald, M. (2022). Deep Learning, Natural Language Processing, and Explainable Artificial Intelligence in the Biomedical Domain. *arXiv preprint arXiv:2202.12678*.
- Murdoch, W. J., Singh, C., Kumbier, K., Abbasi-Asl, R., & Yu, B. (2019). Interpretable machine learning: definitions, methods, and applications. *arXiv preprint arXiv:1901.04592*.
- Nguyen, A., Dosovitskiy, A., Yosinski, J., Brox, T., & Clune, J. (2016). *Synthesizing the preferred inputs for neurons in neural networks via deep generator networks*. Paper presented at the Advances in neural information processing systems.
- Petsiuk, V., Das, A., & Saenko, K. (2018). *RISE: Randomized input sampling for explanation of black-box models*. Paper presented at the the British Machine Vision Conference (BMVC).
- Petsiuk, V., Jain, R., Manjunatha, V., Morariu, V. I., Mehra, A., Ordonez, V., & Saenko, K. (2021). *Black-box explanation of object detectors via saliency maps*. Paper presented at the Proceedings of the IEEE/CVF Conference on Computer Vision and Pattern Recognition.
- Radford, A., Wu, J., Child, R., Luan, D., Amodei, D., & Sutskever, I. (2019). Language models are unsupervised multitask learners. *OpenAI blog*, 1(8), 9.
- Redmon, J., Divvala, S., Girshick, R., & Farhadi, A. (2016). *You only look once: Unified, real-time object detection*. Paper presented at the Proceedings of the IEEE conference on computer vision and pattern recognition.
- Ren, S., He, K., Girshick, R., & Sun, J. (2015). Faster r-cnn: Towards real-time object detection with region proposal networks. *Advances in neural information processing systems*, 28.
- Ribeiro, M. T., Singh, S., & Guestrin, C. (2016). "Why Should I Trust You?": Explaining the Predictions of Any Classifier. Paper presented at the Proceedings of the 22nd ACM SIGKDD International Conference on Knowledge Discovery and Data Mining, San Francisco, California, USA.
- Russell, S. J., & Norvig, P. (2009). *Artificial Intelligence: A Modern Approach (3rd ed.)*. Upper Saddle River, New Jersey: Prentice Hall.
- Yan, Y., Li, X., Zhan, Y., Sun, L., & Zhu, J. (2022). GSM-HM: Generation of Saliency Maps for Black-Box Object Detection Model Based on Hierarchical Masking. *IEEE Access*, 10, 98268-98277. doi: 10.1109/ACCESS.2022.3206379
- Zaidi, S. S. A., Ansari, M. S., Aslam, A., Kanwal, N., Asghar, M., & Lee, B. (2022). A survey of modern deep learning based object detection models. *Digital Signal Processing*, 126, 103514. doi: <https://doi.org/10.1016/j.dsp.2022.103514>
- Zhao, Z. Q., Zheng, P., Xu, S. T., & Wu, X. (2019). Object Detection With Deep Learning: A Review. *IEEE Transactions on Neural Networks and Learning Systems*, 30(11), 3212-3232. doi: 10.1109/TNNLS.2018.2876865
- Zintgraf, L. M., Cohen, T. S., Adel, T., & Welling, M. (2017). Visualizing deep neural network decisions: Prediction difference analysis. *arXiv preprint arXiv:1702.04595*.